Spectroscopic Techniques for Measurement of Velocity and Temperature in the DLR High Enthalpy Shock Tunnel HEG

W. H. Beck
Aerothermodynamics Section,
Institute of Fluid Mechanics,
German Aerospace Center (DLR),
Bunsenstraße 10,
37073 Göttingen
Germany

ABSTRACT

The theory of absorption techniques, including line broadening and shifts, along with a brief description of the spectroscopy of the seed species Rb, will be given. A brief overview of the diode laser itself and the experimental setup for the technique follow. Results are split into two parts: preparatory and calibration work in a test cell and a small test shock tube, followed by results in HEG, are presented. Here time profiles for gas temperature T_{trans} and velocity u are given for various HEG run conditions.

1. INTRODUCTION

As in any wind tunnel, the free stream flow in the High Enthalpy Shock Tunnel HEG of the DLR in Göttingen needs to be characterised (i.e. calibrated) properly in order to carry out measurements on small test models. Standard techniques are bulk techniques, whereby pressures (Pitot or static) and stagnation point heat transfer rates are measured at various radial and axial positions after the nozzle exit, to be then compared with CFD results from which other flow propereties can be calculated. However, this represents experimentally a very limited data set with which to validate the CFD codes - measurement of other physical properties such as gas temperatures (either inner or translational T_{trans}), velocities u and species concentrations are hence highly desirable. For example, a measurement of u is the best way to determine whether the enthalpy of the gas is as high as expected and calculated from shock speed and/or CFD of the nozzle flow. Spectroscopic techniques such as LIF and CARS can deliver rotational T_{rot} and vibrational T_{vib} temperatures, and in some cases also species concentrations. (For the former, one usually *assumes* that $T_{rot} \approx T_{trans}$.) They can't measure T_{trans} or in most cases u.

The aim of this lecture is to present the diode laser absorption technique, which can deliver T_{trans}, u and, depending on the probed species, also concentration by a measurement of line broadening, line shift and line area, respectively. As used on HEG, a seed species rubidium Rb was introduced into the test flow in minute concentrations, thereby not itself influencing the flow properties in any way. Another naturally occurring species in HEG, NO, has also been probed using this technique (Ref. 1), only in that case measurements were performed in the IR, whereas the Rb work was carried out in the visible. The technique has one drawback, however, compared with LIF or CARS; it is a line-of-sight technique, meaning that the signal is integrated over the pathlength of the laser beam through the test region. As will be shown, in the case of HEG, the free stream flow is assumed to be homogeneous in a radial direction, so that this drawback is not severe. The technique in its present form has, therefore, limited applicability to flows where property gradients are large relative to the laser beam path length (e.g. around a test model).

The theory of absorption techniques, including line broadening and shifts, along with a brief description of the spectroscopy of the seed species Rb, will be given. A brief overview of the diode laser itself and the experimental setup for the technique follow. Results are split into two parts: preparatory and calibration work in a test cell and a small test shock tube, followed by results in HEG, are presented. Here time profiles for gas

Paper presented at the RTO AVT Course on "Measurement Techniques for High Enthalpy and Plasma Flows", held in Rhode-Saint-Genèse, Belgium, 25-29 October 1999, and published in RTO EN-8.

temperature T_{trans} and velocity u are given for various HEG run conditions.

2. THEORY

2.1 Absorption spectroscopy

The transmission $T(\bar{\nu})$ of light (wavenumber $\bar{\nu}$) through an absorbing medium is given by the Beer-Lambert law (see Ref. 2, and references therein):

$$T(\bar{\nu}) = \frac{I(\bar{\nu})}{I_0} = e^{-\int k(\bar{\nu})\, d\bar{\nu}},$$

where $I(\bar{\nu})$ and I_0 are the light intensity after and before entering the absorbing medium, respectively, and $k(\bar{\nu})$ is the spectral absorption coefficient. This coefficient can be written as:

$$k(\bar{\nu}) = h \,.\, \bar{\nu} \,.\, n_i \,.\, \frac{B_{ik}}{c} \,.\, \left(1 - e^{-h\bar{\nu}/kT}\right) \,.\, \Phi(\bar{\nu})$$

where h is Planck's constant, n_i the population density in the lower energy level i, B_{ik} the Einstein coefficient for transition from level i to k, c speed of light, k Boltzmann's constant, T the temperature and $\Phi(\bar{\nu})$ the line shape function. This function is the key to the absorption technique; a knowledge of its shape, broadening mechanisms and shift in wavelength will be used to deliver the temperature and velocity of the gas.

2.2 Line broadening

Four mechanisms leading to broadening of absorption will be discussed:

1. Natural linewidth. Although one may expect that the absorption line width for the transition from level i to k, occurring at $\bar{\nu}_0$, is infinitely narrow, this is not possible since it would violate the Heisenberg Uncertainty Principle, one form of which relates the energy uncertainty ΔE_k to the lifetime τ_k of the upper excited state k by $\Delta E_k \cdot \tau_k \geq h/2\pi$. For example, for the lifetime τ_k = 10 ns of the upper state of the Rb D_2 transition ($5^2S_{1/2} \rightarrow 5^2P_{3/2}$, see chapter 2.4 and Fig. 1), the natural line broadening of the Rb absorption line is only 0.5 x 10^{-3} cm^{-1}. Natural line broadening is represented by a Lorentzian line shape.

2. Pressure broadening. Also called collisional broadening, this is brought about by perturbations of the quantum energy states involved in the transition due to collisions, leading to a smearing of the energy levels and therefore a broadening of the lines. It usually only plays a role at high pressures, and is not important at HEG free stream pressures of about 500 Pa. (For comparison, the D_2 line of sodium, which is in the same column of the Periodic Table as Rb and therefore has similar spectroscopic properties, would experience a line broadening at HEG conditions of only $1x10^{-3}$ cm^{-1}.

3. Doppler broadening. This is the major broadening mechanism in the HEG free stream, and is what is used to determine the translational temperature T_{trans} of the gas. It arises from the movement of the absorbing species in directions towards and away from the direction of the laser beam, leading to small Doppler shifts which manifest themselves as line broadening. For Rb at HEG conditions ($T_{trans} \approx 1000$ K), the broadening amounts to about 30 x 10^{-3} cm^{-1}, and so has about 30 times more influence than pressure broadening. Doppler broadening is represented by a Gaussian line shape.

4. Stark broadening. This mechanism is very important in ionised flows or plasmas, where electron concentrations are quite high. As in pressure broadening, a perturbation of the energy levels arises from species-electron collisions, only for these types of collisions their cross sections are much larger. Electron concentrations in HEG are unkown; CFD calculations of the nozzle flow predict very low values, so that, if correct, this mechanism should not play a major role here.

Doppler broadening leads to a Gaussian line shape $g_D(\bar{\nu})$, whose FWHM (full width at half maximum height) line width $\delta\bar{\nu}_D$ is a function of the temperature T of the excited atom:

$$g_D(\bar{\nu}) = \exp\left[-4 \cdot \ln 2 \cdot \frac{(\bar{\nu} - \bar{\nu}_0)^2}{(\delta\bar{\nu}_D)^2}\right],$$

$$\delta\bar{\nu}_D = \frac{2 \cdot \sqrt{2 \cdot R \cdot \ln 2}}{c} \cdot \bar{\nu}_0 \cdot \sqrt{\frac{T}{M}}.$$

R is the universal gas constant, M the atomic weight, other symbols as before. In the above equation, one can see that, apart from some

constants or quantities, $\delta\bar{\nu}_D$ is a function only of $\sqrt{T}$. Hence, by measuring $\delta\bar{\nu}_D$, one can determine the temperature, albeit not very accurately due to the square root dependence. It should be noted that this is measurement of a translational temperature, and as such is independent of the population of the atomic energy levels, and is not plagued by quenching problems (as in LIF).

In fitting experimentally determined line shapes to theoretical profiles, one usually uses a Voigt profile, which is a composite of the Gaussian profile from Doppler broadening and the Lorentz profile from natural broadening. However, since the Doppler broadening is some 30 times stronger than natural broadening (see before), in HEG free stream flows it is sufficient to use just the Gaussian form, as given in the above equations.

2.3 Line shifts

Whereas line broadening delivers information on temperature, a shift in the line position (in wavelength or wavenumber) due to the Doppler effect can give the relative velocity between the moving atom and the laser beam. This Doppler shift is a direct linear function of the velocity u of the atoms and the angle θ between atom velocity vector and laser beam direction:

$$\Delta\bar{\nu}_{line} = \bar{\nu}_0 \cdot \frac{u}{c} \cdot \cos(\theta).$$

For the D_2 line of Rb, and taking the range of HEG free stream velocities (~4300 - 6200 m s^{-1}), quite large line shifts of about 0.11 - 0.16 cm^{-1} would be expected. This makes the velocity determination much more accurate than that for temperature, since these large shifts can be measured quite accurately.

2.4 The rubidium atom Rb

Rb posseses two naturally occurrring isotopes, ^{85}Rb and ^{87}Rb, with relative proportions of 72% and 28%, respectively. Both contribute to the absorption and so they must both be considered in calculating line shapes. As with all alkali metals, Rb possesses a very strong resonant transition where an electron is promoted from an s to a p orbital. This single electron in the 5s orbital leads to a ground state symbol $5^2S_{1/2}$. The next level, an electron in a 5p orbital leads to the state $5^2P_{3/2}$. Both of these levels are further split due to spin/orbit interactions into hyperfine structure levels, designated by a quantum number F. This hyperfine splitting is quite large for the $5^2S_{1/2}$ ground state - 0.1007 cm^{-1} for ^{85}Rb and 0.2262 cm^{-1} for ^{87}Rb - whereas for the excited state $5^2P_{3/2}$ it is only 0.0072 cm^{-1} for ^{85}Rb and 0.0166 cm^{-1} for ^{87}Rb. Fig. 1 shows on the left a term energy level diagram for Rb, with the strong D_2 transition at 780.2 nm indicated. To the right the sublevel structure of both Rb isotopes is shown.

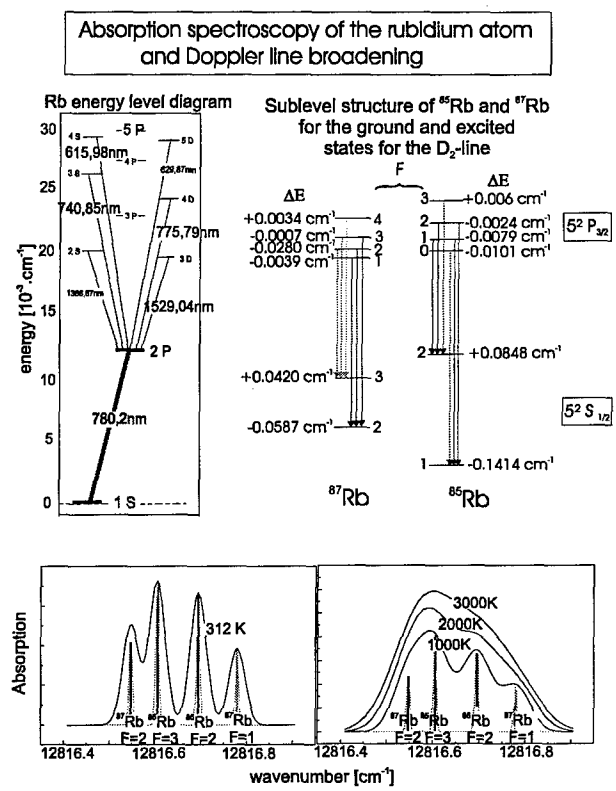

Fig. 1 Energy level diagram and calculated spectra for Rb

With the Doppler broadening to be expected here, transitions from lower states to the upper states F = 0 - 4 cannot be resolved; however, transitions from each of the lower states F = 2, 3 (^{87}Rb) and F = 1,2 (^{85}Rb) can, so that in all four absorption lines will be measured (see calculated spectra in Fig. 1).

The effect of Doppler broadening on the naturally broadened lines can be seen in Fig. 1, lower traces. In both traces the naturally broadened lines have been calculated and are shown in grey; they are designated by the hyperfine level quantum number F from the lower energy level for both isotopes. The left plot shows also calculated Doppler-broadened lines at 312 K; one can see immediately

that the hyperfine structure due the levels F in the upper state merge together, even at this "low" temperature. For higher temperatures, 1500, 2500 and 3500 K, shown right, eventually even these four lines merge into one. It is clear with this example that this method of temperature determination becomes quite inaccurate at higher temperatures, or at the very least requires experimental data of high quality (low S/N).

This broadening as a function of temperature is further exemplified in Fig. 2. Here calculated spectra are shown for temperatures above 3000 K (3000 - 5000 K) and in the range of expected temperatures for HEG free stream flows (700 - 1300 K). Above 3000 K the method is virtually useless! In the range 700 - 1300 K the situation is quite good - it will be shown later that here temperature measurements can be carried out with a (conservative) accuracy of better than ±20%.

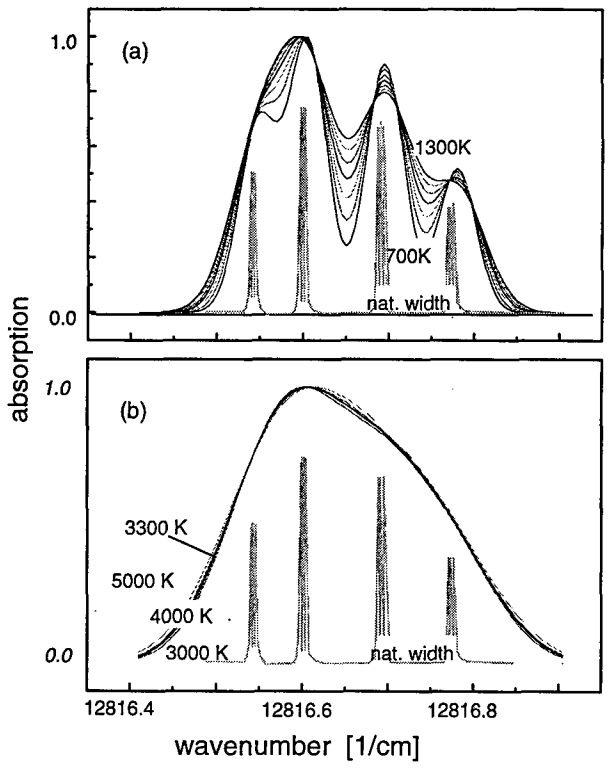

Fig. 2 Calculated Rb spectra (a) 700 - 1300 K; (b) 3000 - 5000 K

3. EXPERIMENTAL TOOLS

3.1 The diode laser

The GaAlAs semi-conductor diode lasers used here are of type III-IV (elements of periodic columns III and IV) and emit in the range 720 - 895 nm. In CW (continuous wave) operation they emit a single longitudinal mode, so that, since their geometry is very small, they have a very narrow bandwidth (~3 x 10^{-3} cm^{-1}). The wavelength of the emitted light is dependent on the temperature and injection current for the diode, although not in a continuous way, but rather step-wise, see Fig. 3.

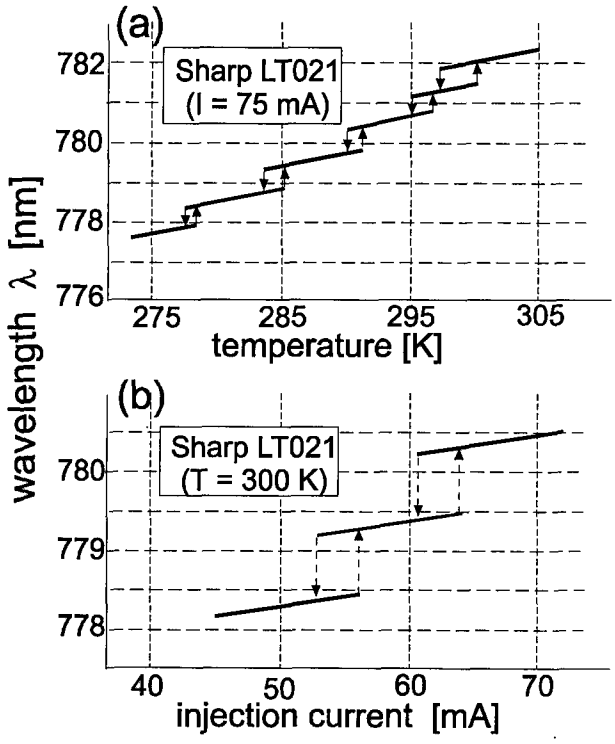

Fig. 3 Dependence of laser diode wavelength on temperature and current

In Fig. 3 the wavelength (in nm) of the emitted light is plotted as a function of (a) temperature (from 275 to 305 K) at constant current, and (b) injection current (from 45 to 70 mA) at constant temperature for Sharp LT021 laser diodes. Wavelength is tunable continuously over a single step over a range of 0.05 to 0.5 nm, depending on laser type; this is wide enough to encompass completely the Rb absorption lines discussed in chapter 2.4. In doing this it is important to be not too close to the edge of one of the steps shown in Fig. 3, otherwise the laser may hop from one mode (step) to another. This can be seen in Fig. 4, where

measured intensity of a ROHM RLD-78NP laser diode is plotted against wavelength for a constant temperature of 15°C and for injection currents between 45.85 and 45.90 mA (in steps of 0.01 mA). The bandwidth of the measured emission is not that of the laser diode, but rather due to the resolving power of the spectrometer used in the measurement.

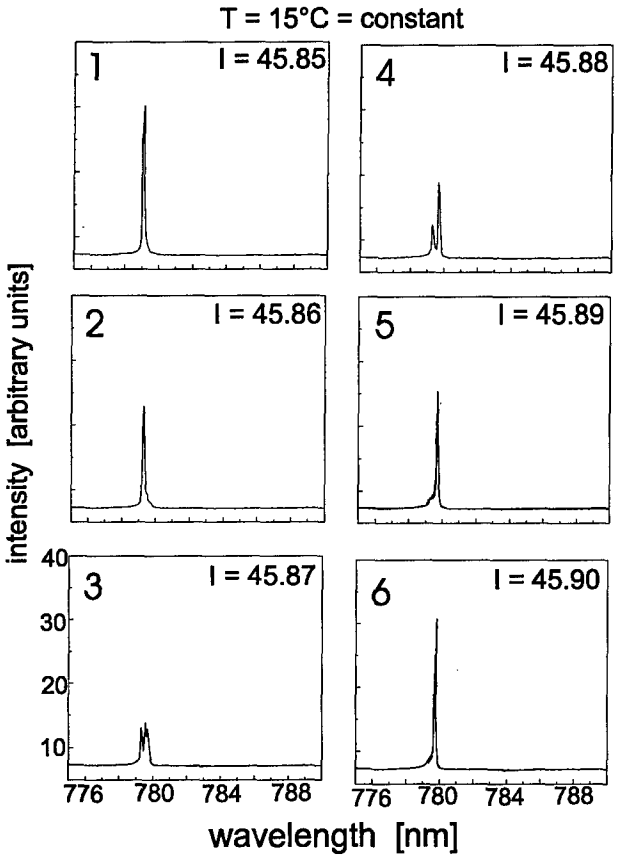

Fig. 4 Laser diode output at different injection currents, showing mode hopping

The figure shows that at currents of 45.87 and 45.88 mA mode hopping must be occurring, so that with the combination of this temperature and these currents, the laser diode is not suitable for scanning work.

Operating conditions which are suitable for Rb absorption work are shown in Fig. 5. At a constant temperature of 281.90 K, a plot of emitted wavelength against injection current is shown. Also included in the figure is the wavelength region (narrow grey region) where the four Rb absorption lines occur. The laser diode mode between 37 and 42 mA nicely encompasses the Rb absorption lines, so that here there is no danger of mode hopping occurring.

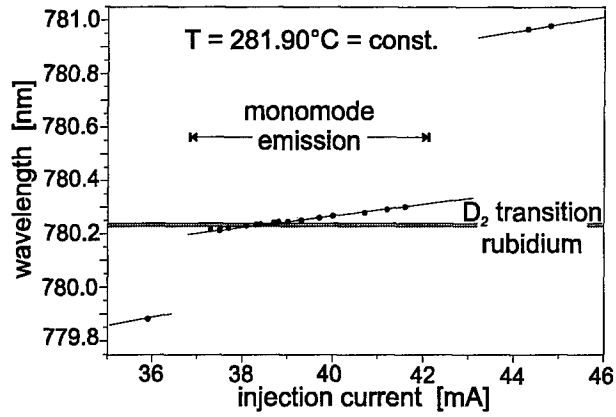

Fig. 5 Single ramp of laser diode output, compared with Rb absorption region

The measurement shown in Fig. 5 was carried out by varying the current step-wise and recording the wavelength. It is also possible to vary this current very rapidly - the laser diode can respond equally rapidly up to 100 kHz. If the injection current is modulated as a sawtooth or triangular function, then the laser will also follow this modulation in both wavelength and intensity of emission. This is done here in measurements on HEG, so that during the available flow test time a multitude of ramps from the triangular-modulated current provide as many absorption spectra, which can each be analysed to give the time dependence of the flow development. (See Ref. 2)

3.2 The rubidium calibration cell

A reference cell is needed to calibrate the wavelength of the laser diode using the accurately known absorption lines of Rb. This cell is made of glass, having a length of 8 cm and a diameter of 1.5 cm, and is sealed at both ends with planar-parallel windows. It is filled with 5 g of high purity Rb und a protective atmosphere of argon. The cell can be heated up to temperatures of 370 K. Rb metal melts at 312 K and has an equilibrium vapour pressure and concentration at this temperature of ~8 x 10^{-5} Pa and ~1.5 x 10^{10} cm^{-3}, respectively. An absorption spectrum of Rb at 273 K recorded with a laser diode is shown in Fig. 6.

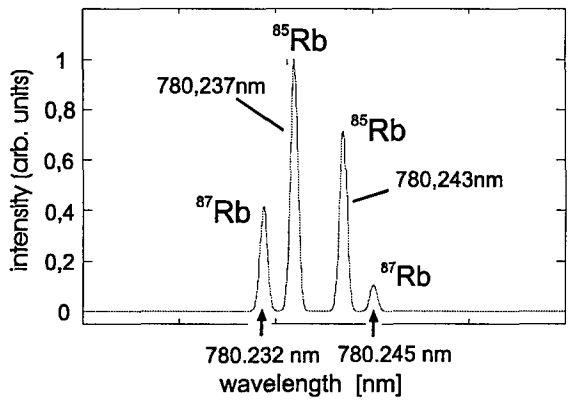

Fig.6 Measured absorption spectrum of Rb using a laser diode

3.3 The test shock tube

Development of the seeding technique, recording of emission spectra and testing of the set-up for recording absorption spectra were all carried out in a small test shock tube. This consists of 1.37 m driver (ø 21.9 cm)and 3.13 m driven (ø 6 cm) tubes separated by a plastic diaphragm. Driver gas was helium at 810 kPa, test gas air or N_2. A small test section (length 13.3 cm) at the end of the driven (shock) tube contains windows for emission and absorption work and pressure sensors. Temperatures here of up to 3000 K were attained.

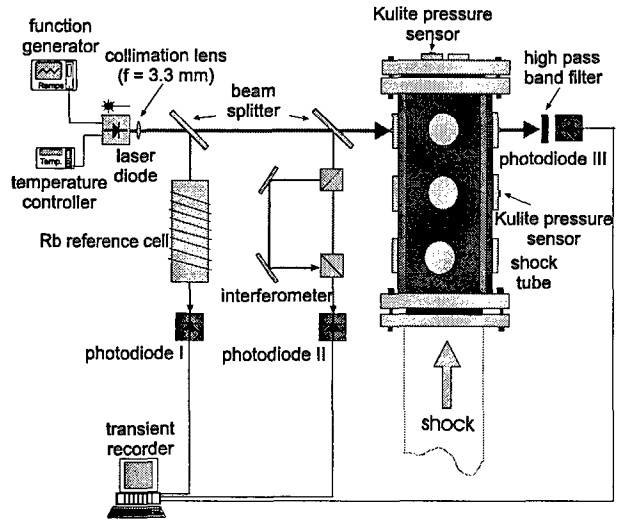

Fig.7 Diode laser absorption setup on the small test tube

The experimental set-up at the test shock tube is shown in Fig. 7. Small portions of the diode laser beam are split off and sent through the reference cell and to an interferometer, where the two beams are recorded by two photodiodes. (The interferometer provides a wavelength calibration over the laser diode scanning range, i.e. one ramp of the triangular modulation.) The main part of the beam passes through the shock tube test section, where it also is recorded by a photodiode. All photodiode outputs are stored in a transient recorder.

3.4 The high enthalpy shock tunnel HEG

The HEG is a free-piston driven shock tunnel operating in the reflected shock mode. It has been described in greater detail elsewhere (ref. 3). As shown in Fig. 8, a reflected shock creates high temperature and pressure conditions in the reservoir (before the nozzle entrance), after which the test gas expands through the nozzle to deliver the free stream conditions in the test section. The test time is about 1 ms. Also shown in Fig. 8 are nominal conditions which have been calculated using a non-equilibrium Euler code for the free stream and the reservoir - these conditions apply to the old contoured nozzle in HEG, with which most of the testing was carried out. Conditions I and III are low pressure, with high and low specific enthalpy, respectively, and II and IV are high pressure, also with respectively high and low enthalpies. Free stream temperatures are calculated to lie between about 500 and 1100 K and flow velocities between 4800 and 6200 m s^{-1}.

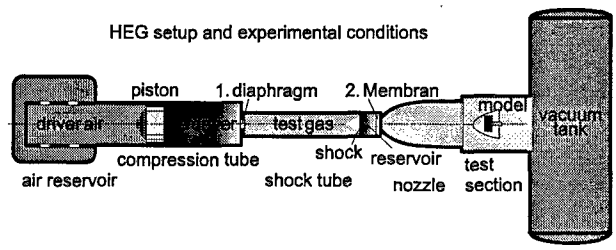

Nominal conditions for the contoured nozzle

Conditons		I	II	III	IV
p_0	[MPa]	40	90	45	110
T_0	[K]	9100	9700	7300	8100
T_∞	[K]	790	1040	550	720
h_0	[MJ/kg]	21	22	13	15
u_∞	[km/s]	5,9	6,2	4,8	5,1
N2	[10^{15}cm^{-3}]	26,1	56,6	44,0	95,6
O2	[10^{15}cm^{-3}]	1,1	4,3	7,6	18,0
NO	[10^{15}cm^{-3}]	1,1	3,0	3,9	8,4

Fig.8 The high enthalpy shock tunnel HEG

3.5 Diode laser set-up on HEG

The set-up for HEG is shown in Fig. 9.

The basic set-up is as in Fig. 7, except that the beam is split into two halves, one of which passes through the HEG test section at 90° and the other at 53° to the flow. Photodiodes I - IV record laser beam signals through the reference cell, the interferometer, and the HEG test section at 90° and at 53°, respectively. Inset plots upper left and mid right show the intensity of the laser output as a function of time (i.e. wavelength) with and without absorption by Rb. Upper right are two emission spectra recorded in HEG with and without seeding with Rb (see chapter 5.1).

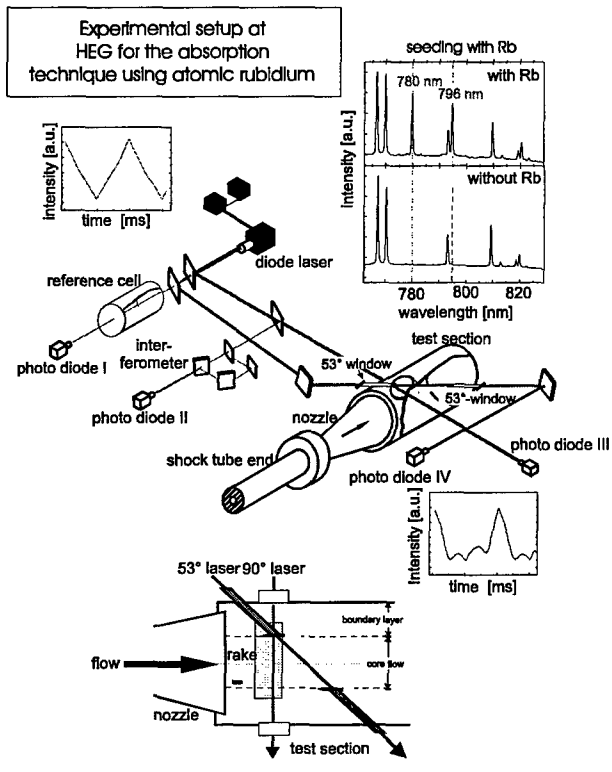

Fig. 9 Diode laser setup in HEG

To avoid influences on the measurement from boundary layer effects (remembering that the technique is line-of-sight integrating), the 53° laser beam path is protected by light guiding pipes, as shown at the bottom of Fig. 9. Here the laser beam "sees" only the core flow. This is shown graphically in Fig. 10.

Here calculated radial profiles at the HEG nozzle exit for temperature and velocity are shown (Ref. 4). The core flow and boundary layer regions are indicated at the top, as are the regions excluded by use of the light guiding pipes. These regions are characterised by very high temperatures and a negative velocity gradient.

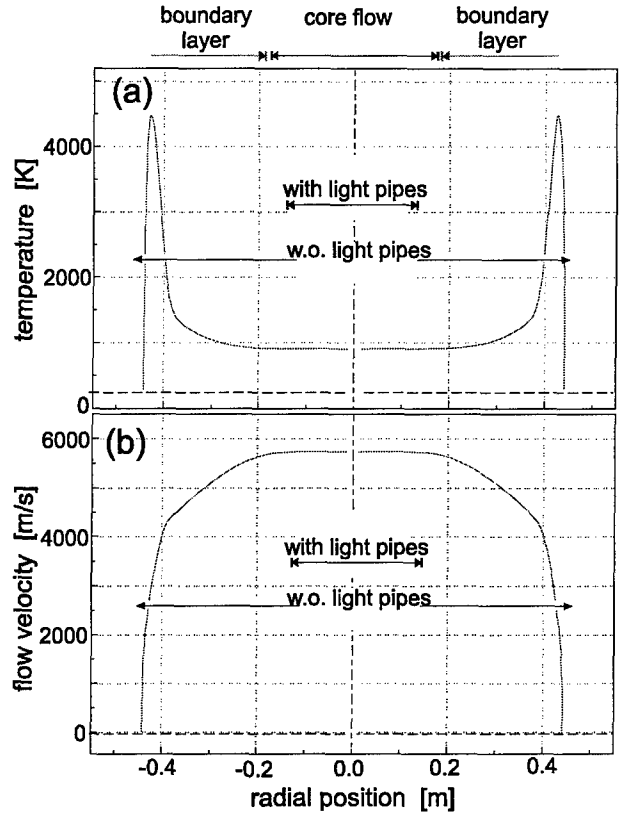

Fig.10 HEG radial temperature (a) and velocity (b) profiles, showing exclusion of boundary layer effects by the light pipes

3.6 Seeding Rb in HEG

Rb is a reactive alkali metal, is not stable in air and so is not suited to be used directly and quantitatively as a seed species. However, its nitrate $RbNO_3$ is readily water soluble and decomposes to its oxide Rb_2O at 550 K, which itself melts at 1500 K. At the high temperatures in the HEG reservoir (up to 9700 K), Rb_2O further decomposes within the flow time to its constituent parts, including atomic Rb. Seeding was carried out with very low concentrations of $RbNO_3$ in water by applying the solution with a brush to surfaces both at the shock tube end and in the compression tube near the diaphragm position (see Fig. 8). Total Rb amounts were around only 1 µg!

4. RESULTS IN THE TEST SHOCK TUBE

Fig. 11 shows a typical shock tube result (test gas air), with: (a) photodiode I signal with Rb absorption in the reference cell; (b) photodiode signal III with Rb absorption in the shock tube; (c) pressures measured at shock tube test section end and side walls. In (b) one can clearly see the initial undisturbed triangular emission trace of the laser diode, followed after arrival of the reflected shock at the test window by superimposed absorption peaks due to Rb. (The gas behind the incident shock in this run was too low to vaporise the Rb_2O, explaining the absence of an absorption signal here.)

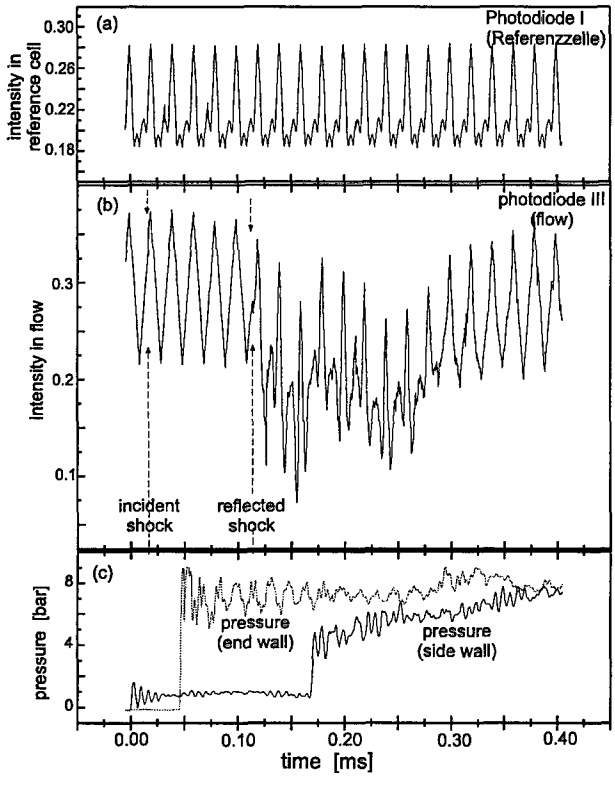

Fig. 11 Measurement in small test shock tube: (a) reference; (b) shock tube ;(c) pressures

The reflected shock region should have a temperature of about 3300 K, according to calculations derived from the shock tube fill pressure and shock Mach number. One of the spectra (one of the ramps) shown in Fig. 11 in the reflected shock regime, after appropriate correction for changing laser beam intensity and conversion to absorption units, is shown in Fig. 12 (dark line plot). Superimposed are calculated (simulated) spectra for temperatures 3000, 3500, 4000 and 4500 K. (For reference, a spectrum for 312 K is also plotted.)

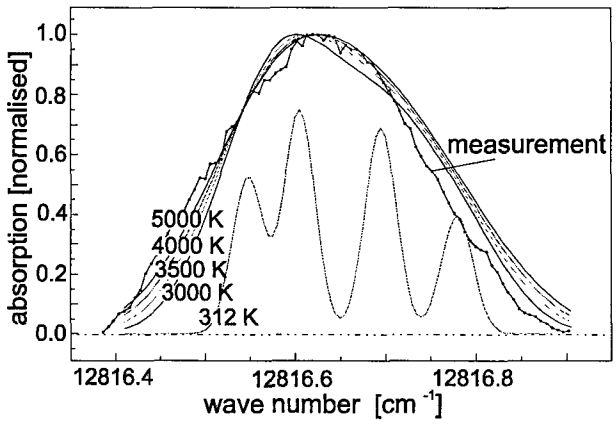

Fig. 12 Comparison of measured and calculated absorption profiles in the test shock tube

One sees here a confirmation of the problem referred to in Fig. 2; the differences between the simulated spectra for this wide temperature range are too small to be resolved by the available experimental data. At these temperatures the method is very inaccurate and not suited.

5. RESULTS IN HEG

5.1 Emission spectra

In order to analyse absorption spectra recorded in HEG correctly, one needs to be sure that absorption is occurring only through the presence of Rb, and not overlapped by other disturbing absorbing species. Before the first introduction of Rb into HEG, emission spectra in front of a flat plate (of area 20 cm^2) placed in the HEG test section normal to the flow direction were recorded using an optical multichannel analyser. The reservoir region was then seeded and another spectrum recorded. Both spectra were shown in Fig. 9, upper right. Here it is clear that the only emitting (and therefore absorbing) species at 780.2 nm is Rb.

5.2 Seeding results

Core vs boundary layer regions. After the first seeding experiment, there remain for future shots always small amounts of Rb compounds at the shock tube end and nozzle inlet, present as "dirt" on the walls. This Rb does not enter the core

region, as can be seen in Fig. 13(b). Shown in this figure for a shot at condition I are (a) Pitot pressure in the test section; (b) Absorption from an experiment without prior Rb seeding for both 90° and 53° laser beams, where the latter was protected by the light guiding pipes; (c) Absorption for 53° laser beam from an experiment where Rb was seeded into the flow (dark line trace), compared with the unseeded experiment (grey).

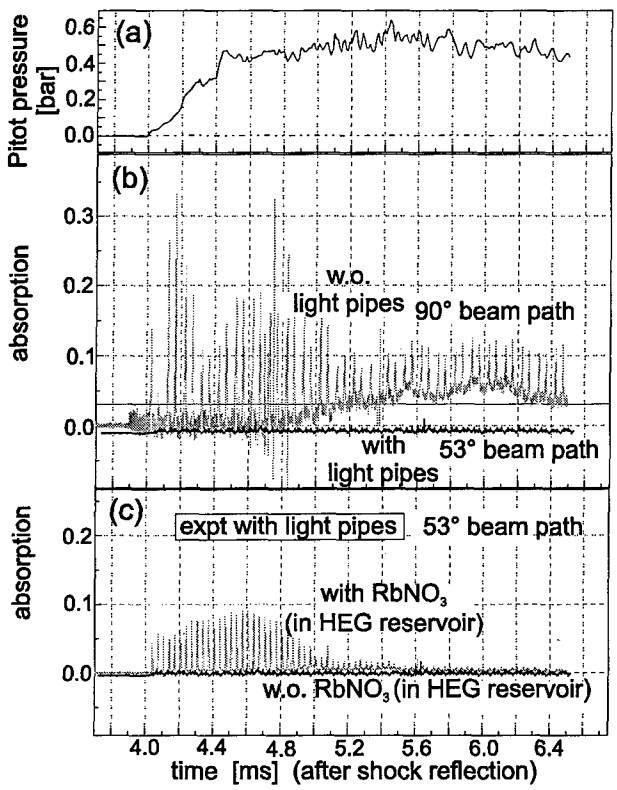

Fig. 13 Rb absorption spectra in HEG, showing contributions of core and boundary layer regions

(b) shows clearly that for the unseeded experiment, the only Rb absorption signal is in the boundary layer region outside the core flow, due to the dirt. This absorption also persists for quite long times - >2.5 ms after flow arrival. In the case of Rb seeded immediately before the shot (upper trace in (c)), there is absorption from the core region for the 53° laser beam; this Rb does not remain very long (<1 ms).

This effect can be further clearly seen in Fig. 14, where both laser beam transmission traces ((a) and (b)) are shown plotted versus time for an HEG shot at condition I (as before, in Fig. 13, gas arrival occurs at about 4.0 ms). Note how the absorption from the unprotected 90° laser beam persists for a long time. A small time excerpt from both traces (a) and (b) for the time window 4.875 - 5.00 ms is shown in (c). The Doppler shift of the 53° laser beam absorption spectrum relative to that for the 53° beam is obvious. This will be analysed later (chapter 5.4).

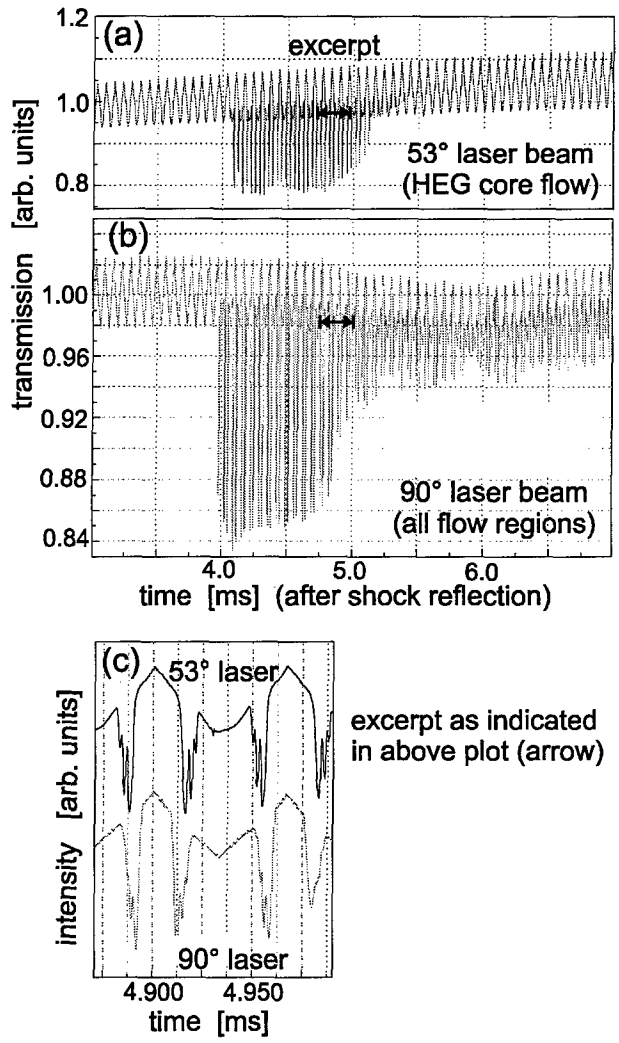

Fig. 14 Rb absorption spectra in HEG (as in Fig.13), showing Doppler-shifted absorption lines

Quantity of seeded species. The influence of quantity of seeded species can be seen in Fig. 15. Both absorption results (a) and (b) were carried out at the same HEG run condition I, only the quantity of $RbNO_3$ seeded into the flow in the reservoir was different; (a) 0.15 µg , and (b) 2.0 µg. Both absorption axes are plotted to the same scale, allowing a direct comparison. (Pitot pressure traces are shown for reference at the top of (a) and (b).)

Note that in both cases there is little Rb left during the indicated test window.

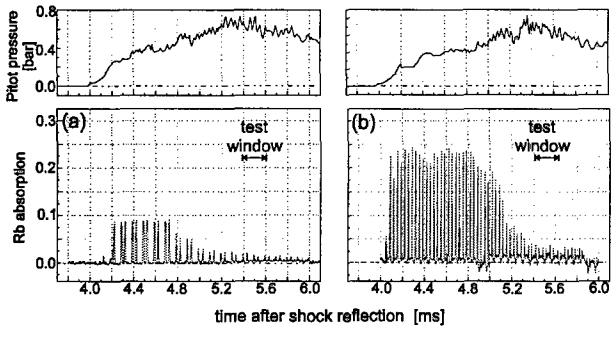

Fig. 15 Effect of Rb seeding amounts on absorption spectra: (a) 0.15μg; (b) 2.0μg

Seeding in shock vs compression tubes. Fig. 16 compares the result shown in Fig. 15 with 0.15 μg $RbNO_3$ seeded into the reservoir (dark grey trace) with a result where 5.0 μg $RbNO_3$ were seeded into the flow upstream of the diaphragm in the compression tube (light grey). Both shots were at condition I. Both traces have a similar form until about 4.5 ms, after which a new charge of Rb, originating from the compression tube, enters the probed region (light grey trace).

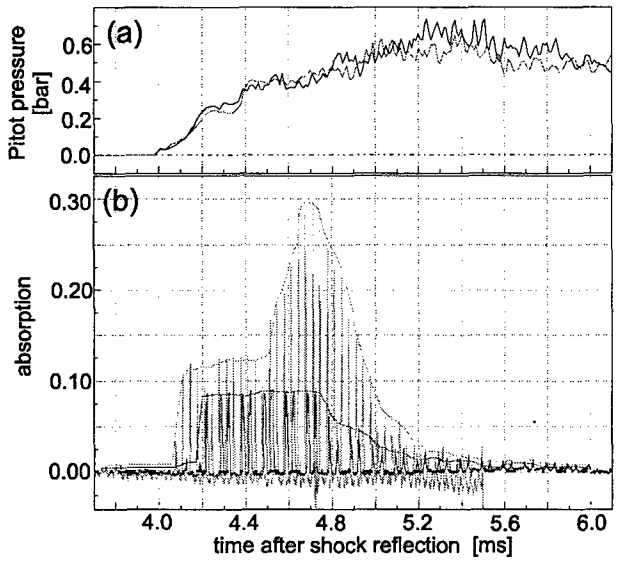

Fig. 16 Effect of seeding in shock and compression tubes: (a) pressure; (b) absorption

Since the Rb seeded in the compression tube can only be carried downstream by the helium driver gas, its presence thus signals the arrival of the first He in the test gas at about 4.5 ms. This early arrival of He has since been confirmed by other techniques and by CFD. Furthermore, in both results there are only weak absorption signals at later times, making analysis difficult. The main advantage of the seeding in the compression tube is to spread the Rb (as some compound) through the *whole* shock tube, so that for the following shots the *whole* test gas (air) slug is seeded more or less equally.

5.3 Time-resolved absorption measurements in HEG

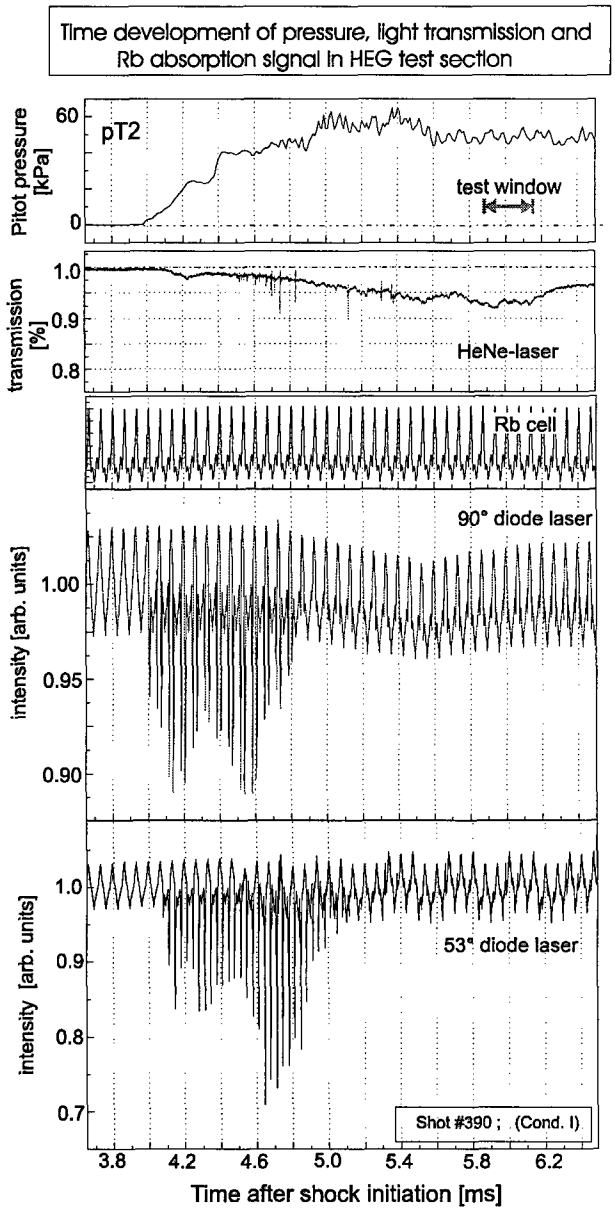

Fig. 17 Rb absorption in HEG at condition I (see text)

The time development of Rb absorption in a typical condition I shot, such as will be used later in an analysis for temperature and velocity, is shown in Fig. 17. Plotted from top to bottom are:

Pitot pressure pT2, showing the test window; extinction measurement through the HEG test section using a HeNe laser beam; reference Rb absorption spectrum from the calibration cell; absorption spectrum in HEG with 90° laser beam; absorption spectrum in HEG with 53° laser beam.

Note that for this shot condition there is at most a laser beam extinction of about 7%. This is quite small, but nevertheless the laser diode beam transmission traces need to be corrected for this. At higher shot pressures (conditions II and IV) the extinction is much larger, making the correction more difficult and the result less accurate. (There are no species here that absorb at the HeNe laser wavelength, so that this measured extinction is thought to be due to particulate matter in the flow.)

5.4 Determination of line broadening and shifts

Line broadening. Two of the many ramps that were shown in Fig. 17 for the 53° laser beam absorption result are shown in Fig. 18(a). Here two absorption spectra are plotted overlapped with zero absorption spectral traces (used for base line correction). For reference, a typical interferometer trace is also shown (used for wavelength linearity check over the ramp). After applying base line and linearity corrections, and converting to a scale in units of absorption, the experimental trace (grey curve) shown in Fig. 18(b) is obtained. A χ^2-fitting procedure with temperature T_{trans} as fit parameter is then used to fit the theoretical (Gaussian) lineshape function, as discussed in chapter 2.2, to the experimental trace. This result is also shown in the figure (dark trace). The resulting temperature is T_{trans} = 1120 ± 300 K; even at these lower temperatures, the method is not very accurate.

Line shifts. Even though the 90° laser beam cannot be used to deliver useful temperatures (they represent an average integrated over different flow regions, see Fig. 10), it does however provide a very useful reference for line shifts in the 53° laser beam spectra. Two such absorption spectra from both laser beams (shown in Fig.17) are plotted overlapped on the same axis in Fig. 19.

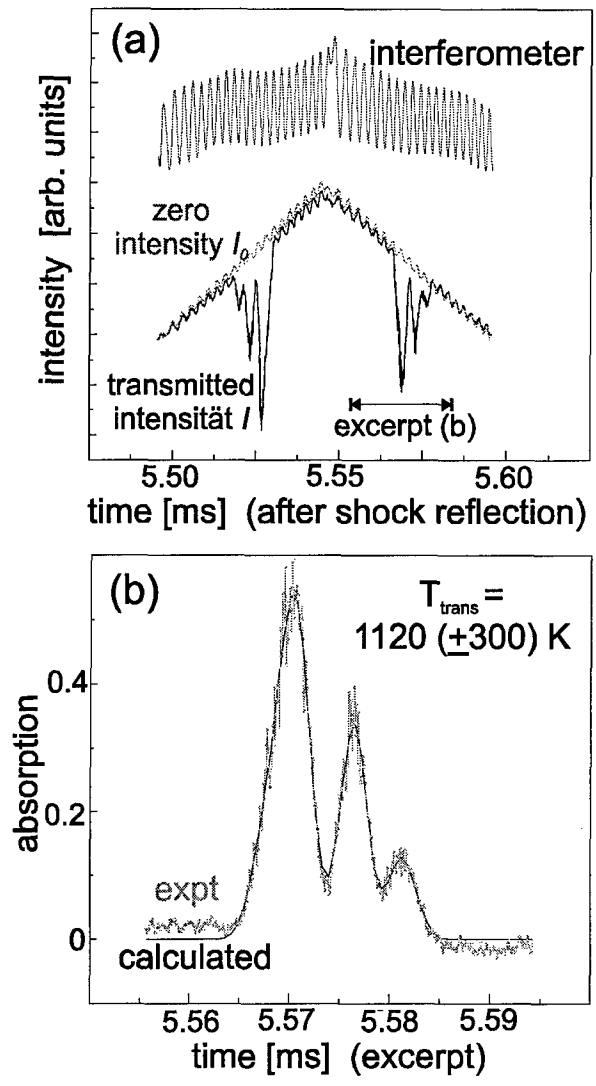

Fig. 18 Measured single Rb absorption spectra in HEG: (a) Two ramps; (b) comparison with theory

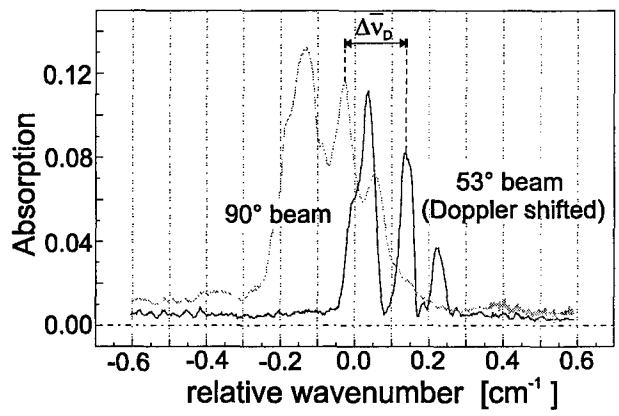

Fig. 19 Orthogonal and 53° Doppler-shifted Rb absorption spectra in HEG

The abscissa is in units of line shift in wavenumbers, taken relative to an arbitrary origin. The line shift $\Delta\bar{\nu}_D$ was measured às 0.1638 ± 0.0035 cm^{-1}. Using the method outlined in chapter 2.3, a flow velocity of 6370 ± 130 m s^{-1} could be determined.

5.5 Accuracy of measurements (goodness of fit)

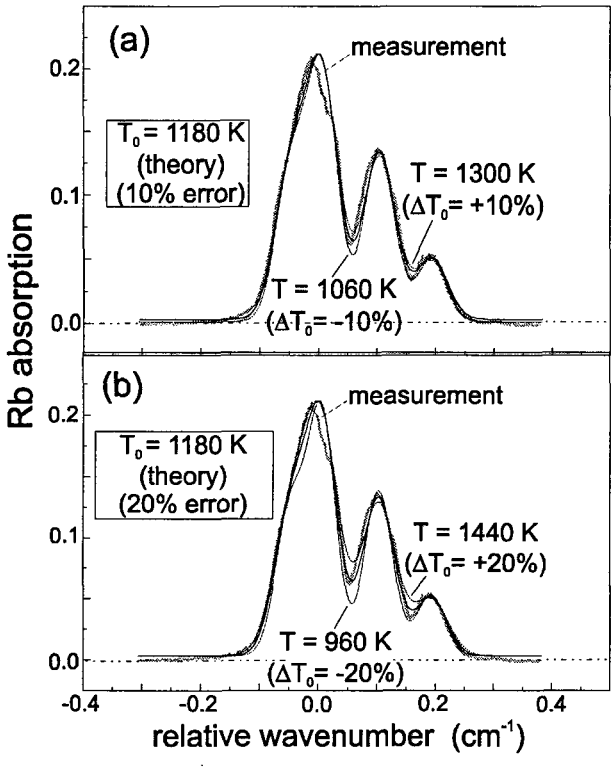

Fig. 20 Comparison of measured and theoretical absorption spectra in HEG, with temperature ranges of ±10% (a) and ±20% (b)

The accuracy of the results of temperature and flow velocity presented in chapter 5.4 for a typical spectrum is limited in part due to considerations already discussed beforehand (chapters 2.2 and 2.3). This will be clarified by a few further examples.

Figs. 20 and 21 show measured Rb absorption spectra compared with simulated spectra for temperature ranges of ±10% and ±20% (Fig. 20) and a velocity range of ±5% (Fig. 21). It can clearly be seen that velocity fits are more accurate than temperature fits.

This is further exemplified by the ±5% χ^2 plots for temperature and velocity shown in Fig. 22. Note here also the difference in ordinate scales for temperature and velocity!

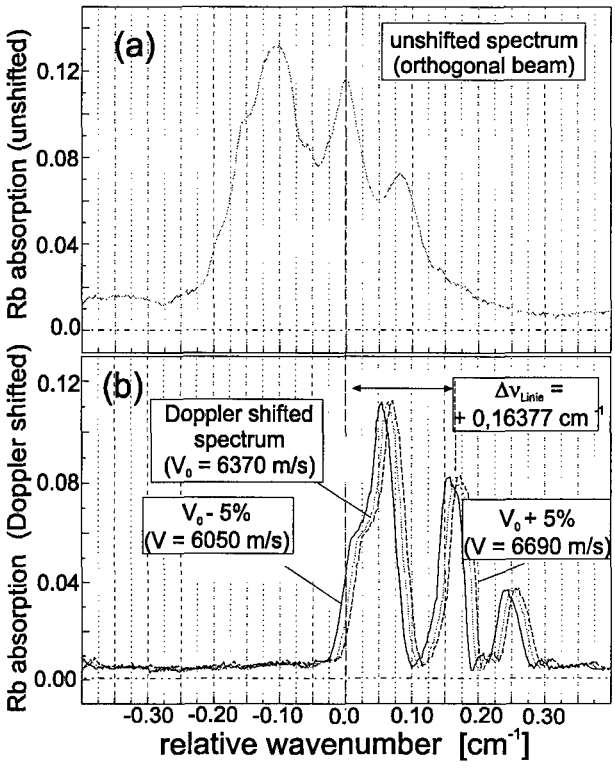

Fig. 21 Unshifted (a) and shifted (b) measured spectra, compared with theoretical spectrum for velocity range of ±5%

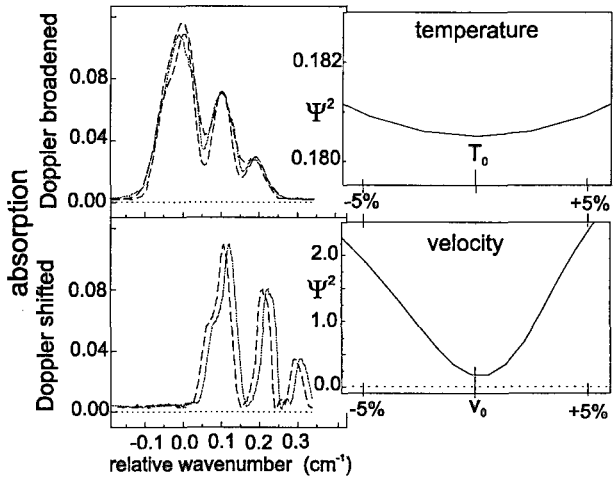

Fig. 22 χ^2 plots for temperature and velocity, showing relative sensitivity of both

5.6 Temperatures and velocities in the HEG free stream

Fig. 23 shows a comparison between experimental and simulated absorption plots for HEG shot 390 (condition I). The agreement is very good.

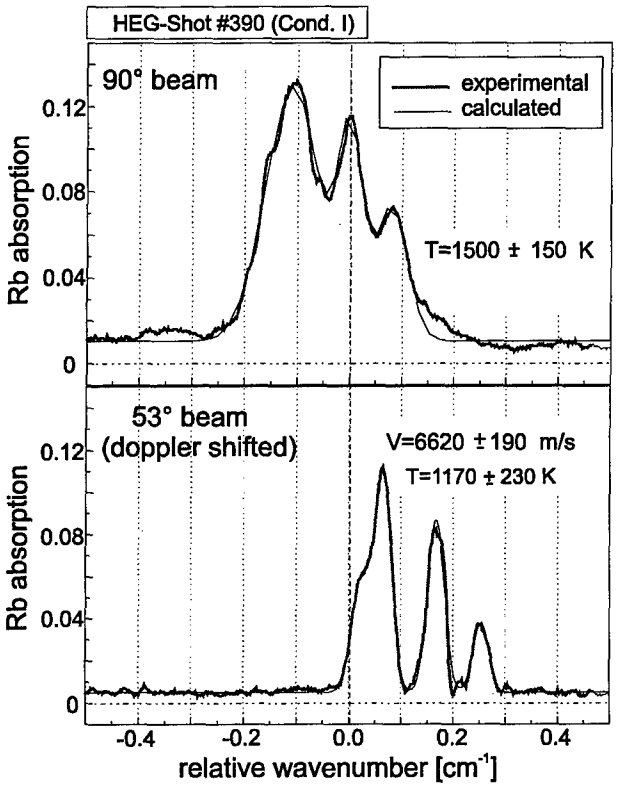

Fig.23 Comparison of measured and simulated spectra for 90° and 53° beams in HEG

When all spectra obtained during the duration of the flow test time in shot 390 are analysed in a similar way, one obtains the time-dependent development of temperature and flow velocity, as shown in Fig. 24. From top to bottom are shown: Pitot pressure trace in the test section (for reference, the test window is also shown); Raw absorption trace for the 53° laser beam; Temperature and velocity time profiles for two cases, with and without positioning of a measurement rake in the test section. (These studies were carried out during calibration measurements of the HEG free stream flow using a rake in the form of a cross equipped with pressure and temperature sensors and placed at the nozzle exit - this could lead to some disturbances in the downstream region, over some of which the 53° laser beam passed.)

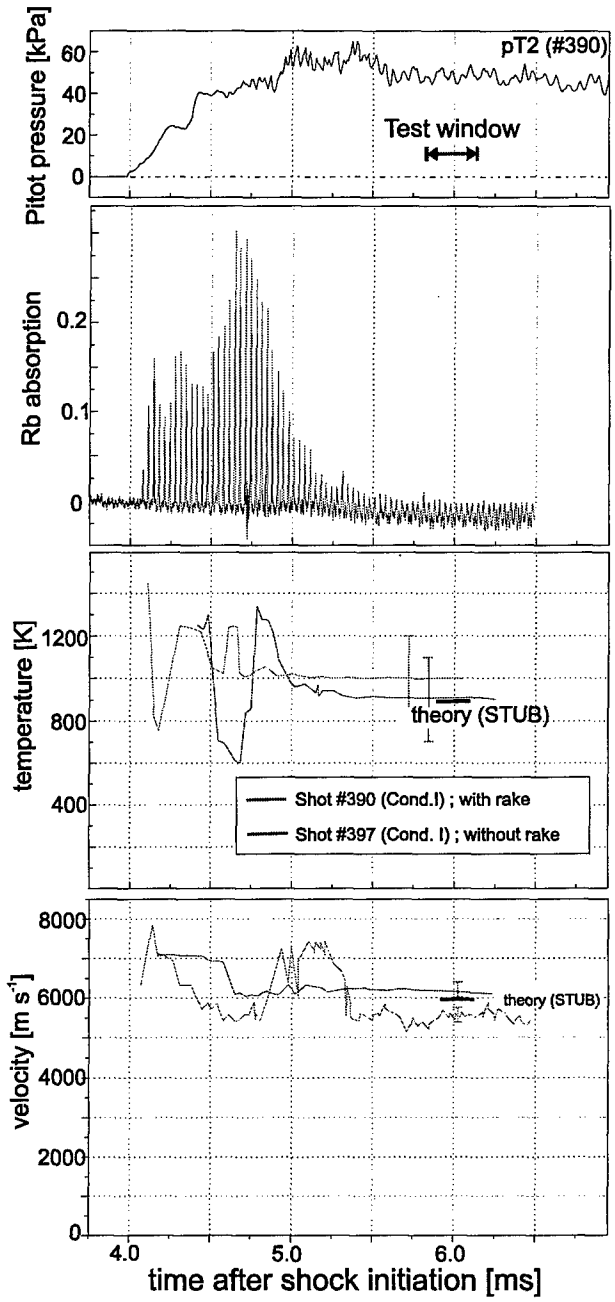

Fig.24 Time development of temperature and velocity in HEG at condition I

Values of temperature and velocity calculated using an Euler chemical non-equilibrium code (STUB) for the HEG nozzle flow are also shown. Both temperature and velocity traces show considerable oscillation at early times when the flow is still being established. With the rake, velocities are lower and temperatures are higher. This is as expected if the measurement rake blocks some of the flow. However, there were too few shots carried out with and without rake to be certain of its influence.

The results obtained from all HEG shots (at conditions I, II, IV, V and VI) are summarised in the following table. Shown is the measured value of temperature and velocity, taken as the average value in the time plots over the designated test time window (as shown in Fig. 24) Theoretical values from STUB, and the differences between STUB and measured values are also shown.

Cond.	T_{expt} (K)	T_{STUB} (K)	ΔT (%)	u_{expt} (m s^{-1})	u_{STUB} (m s^{-1})	Δu (%)
I	1000	807	+24	5600	5939	-6
II	1410	1036	+36	5500	6157	-11
IV	1100	722	+52	3900	5148	-24
V	1010	503	+100 !	4100	4382	-7
VI	910	536	+70	3830	4582	-20

Temperature values lie systematically above the theoretical results (in one case, 100%! higher), velocities systematically below. The differences between experiment and theory in the velocities are much less than with the temperatures; this is not unexpected, in view of the discussions on accuracy of this method. Furthermore, the simplified approach taken in the Euler calculations may also be suspect and would definitely be more reliable using a full non-equilibrium (thermal and chemical) Navier-Stokes solution. Since the differences between measured and theoretical results are in the right direction to be explained by the presence of the measurement rake, more results in a non-disturbed free stream are needed.

ACKNOWLEDGEMENTS

This technique was implemented at HEG initially by Dr. W. Gillespie to look at O atom absorption. The rubidium seeding technique was developed and all subsequent tests in HEG were carried out by O. Trinks in the framework of his Diplom thesis; this thesis forms the basis for this lecture. Financial support of the ESA through CNES for much of the testing is gratefully acknowledged.

REFERENCES

1. Mohamed A.K., Henry D., Bize D. and Beck W.H. (1998) Infrared Diode Laser Measurements in the HEG Free Stream Flow, *AIAA Paper 98-2870.*

2. Trinks O. and Beck W.H. (1998) Application of diode-laser-absorption technique with the D_2 transition of atomic Rb for hypersonic flow-field measurements, *Appl. Optics 37 (30), 1-6.*

3. Eitelberg G. (1993) Calibration of the HEG and its Use for Verification of Real Gas Effects in High Enthalpy Flows, *AIAA Paper 93-5170.*

4. Hannemann K. (1997) *Private communication.*